Wavelength tunable soliton rains in a nanotube-mode locked Tm-doped fiber laser

B. Fu,[1,2,3] D. Popa,[1] Z. Zhao,[1] S. A. Hussain,[1] E. Flahaut,[4] T. Hasan,[1] G. Soavi,[1] and A. C. Ferrari[1,a)]
[1]*Cambridge Graphene Centre, University of Cambridge, Cambridge CB3 0FA, United Kingdom*
[2]*Beijing Advanced Innovation Center for Big Data-Based Precision Medicine, Beihang University, Beijing 100191, China*
[3]*School of Instrumentation and Optoelectronic Engineering, Beihang University, Beijing 100191, China*
[4]*University Paul Sabatier, CIRIMAT/LCMIE, CNRS UMR 5085, Toulouse, France*

(Received 7 July 2018; accepted 13 October 2018; published online 7 November 2018)

We report soliton rains in a tunable Tm-doped fiber laser mode locked by carbon nanotubes. We also detect their second- and third-harmonics. We achieve a tunability of over 56 nm, from 1877 to 1933 nm, by introducing a polarization-maintaining isolator and two in-line polarization controllers. This makes our system promising as a tunable filter for ultrafast spectroscopy. *Published by AIP Publishing.* https://doi.org/10.1063/1.5047492

Soliton rains (SRs) in mode-locked fiber lasers are drifting pulses generated from the continuous wave (CW) background noise[1,2] or the condensed phase (CP) (i.e., a static pulse instead of drifting ones).[3–6] These drift towards the next adjacent CP spontaneously.[1–8] They were first reported in Refs. 1 and 2 and, since then, in many other mode-locked fiber lasers.[3–8] SRs are characterized by 3 properties: drift, CP, and CW background noise.[1,2] SRs were first reported in Er-doped fiber lasers,[1,2] generated from the CW background noise and drifting towards the CP, triggered by the injection of an external CW laser.[1,2] SRs were also generated from the CP in a normal dispersion Yb-doped fiber laser with a dual-filter effect,[3] providing insights into the dissipative SR dynamics.[3] Dispersion and nonlinearity are the main factors responsible for the difference of soliton dynamics because an intracavity pulse is shaped by a balance of cavity dispersion and pulse-triggered nonlinear effects.[9] The dispersion of the cavity is different at different wavelengths. At 1 μm, the dispersions of Yb-doped and single mode fibers (SMFs) are positive.[3–5] Therefore, the lasers operate in normal dispersion, leading to dissipative soliton mode-locking.[3–5] The soliton pulses are formed by a spectral filtering effect.[3] At 1.5 μm in Er-doped fiber lasers, the Er-doped fiber dispersion is positive[1,2,6,7] and that of SMF is negative.[1,2,6,7] The laser thus operates either in normal or anomalous dispersion, as determined by the net dispersion of gain fiber and SMF.[1–7] In this case, the soliton pulses are shaped by a balance of cavity dispersion and pulse-triggered nonlinear effects.[1,2,6,7] At 2 μm in Tm-doped fiber lasers, the dispersions of Tm-doped fiber and SMF are negative.[8,10] The lasers operate in anomalous dispersion[8,10] and usually need a filter to achieve soliton pulses.[10] SRs have been studied at 1 μm (all-normal dispersion Yb-doped fiber laser[3–5]) and 1.5 μm (anomalous dispersion Er-doped fiber laser,[1,2,6,7] as determined by the net dispersion of gain fiber and SMF[1,2,6,7]) with one report at 2 μm (anomalous dispersion Tm-doped fiber laser[8]) based on a nonlinear amplified loop mirror cavity.[8] Reference 8 exploited a two-ring design with a rather long cavity (116 m) compared to standard (~10 m) soliton fiber lasers.[1–7] The signal-to-noise ratio (SNR) was ~50 dB (i.e., ~10^5), much lower than that in Tm-doped standard (~10 m) soliton fiber lasers,[10] where it is ~70 dB (i.e., ~10^7). This means that the mode-locking in Ref. 8 is not as stable as that in Ref. 10. Furthermore, there is no SR report to date in a wavelength tunable laser. Therefore, to better understand the soliton dynamics in wavelength tunable SR lasers, it is necessary to find simple, wavelength tunable methods able to support SRs in Tm-doped fiber lasers. Tm-doped fiber lasers can operate in the 2 μm region, which is eye-safe, because liquid water (main constituent of human tissues) absorbs strongly.[11] These have potential applications in molecular spectroscopy,[12] optical communications,[13] medicine,[14] and light detection and ranging (LIDAR).[15]

Here, we report soliton rains in a broadband wavelength tunable Tm-doped fiber laser mode-locked by a carbon nanotube (CNT) saturable absorber (SA). The second- and third-harmonic SRs are also observed. A polarization-maintaining isolator (PM-ISO) along with two polarization controllers (PCs) is used as a birefringence filter,[16] enabling wavelength tunable soliton pulses from 1877 to 1933 nm, making this promising as a tunable filter for ultrafast spectroscopy.

CNTs can be used as SAs for mode-locking,[17–25] as they provide high modulation depths [~17% (Ref. 23)], preferred for mode-locked fiber lasers,[17–25] typically operating with higher gain and cavity losses than their solid-state counterparts,[26] and larger than those usually reported for graphene devices.[25,27,28] Transition metal dichalcogenides can be used as SA at 2 μm.[29,30] However, Refs. 29 and 30 did not report SRs nor tunable wavelengths. Here, we use solution processed CNTs to fabricate the SAs.[24] ~0.03 wt. % purified laser ablation single-wall CNTs[31,32] and ~0.02 wt. % of purified catalytic CVD grown double-wall CNTs (DWNTs)[33] are ultrasonicated separately for an hour with ~0.7 wt. % sodium-carboxymethylcellulose (Na-CMC) using a tip sonicator at 100 W and 10 °C for 4 h. The dispersions are then ultra-centrifuged. The topmost ~60% is decanted, mixed, ultrasonicated again for 30 min, and then drop-cast, and the solvent evaporated in a desiccator, resulting in a ~30 μm thick CNT-CMC composite. The mean inner and

a)Author to whom correspondence should be addressed: acf26@cam.ac.uk

outer diameters of the DWNTs are ~1.1 and 1.8 nm,[20] resulting in absorption peaks at ~1.1 and 1.9 μm.[20,34]

A schematic of our Tm-doped fiber laser setup is shown in Fig. 1. It consists of a 2.9 m Tm-doped fiber (TDF, SCF-TM-8/125), with a group velocity dispersion (GVD) ~69 ps^2/km at 1900 nm, a wavelength-division multiplexer (WDM) to couple the pump source [1560 nm laser diode (LD) amplified by an Er-doped fiber amplifier, EDFA] into the TDF, a polarization-maintaining isolator (PM-ISO, 0.81 m PM 1550 fiber pigtail) to ensure unidirectional operation, two in-line polarization controllers (PCs), and an optical coupler with a 20% output. The CNT-SA is sandwiched between the two fiber ferrules. The rest of the cavity is ~8 m standard single-mode fiber (SMF-28, with GVD ~67 ps^2/km at 1900 nm), and the total cavity length is ~11.7 m. The total dispersion is ~−0.79 ps^2. The output is monitored by an optical spectrum analyzer, a 4 GHz oscilloscope (Infiniium MSO9404A) with a 10 GHz extended InGaAs photodetector (Newport 818-BB-50), an autocorrelator, a spectrum analyzer, and a power meter.

Mode-locking self-starts when the pump power reaches ~500 mW. The output power is 16.3 mW, and the pulse energy is 0.92 nJ. As shown in Fig. 2(a), the central wavelength is 1893 nm with a full width at half maximum (FWHM) ~14.5 nm. The arrows in Fig. 2(a) indicate the 8 nm wavelength spacing caused by the Lyot birefringence filter effect,[16] attributed to the two PCs and the PM-ISO. This can be calculated as $\Delta\lambda = \lambda^2/(L\Delta n)$,[16] where L is the length of the PM fiber and Δn is the modal birefringence. The PM fiber length can affect the pulse duration.[35] However, we can more easily get tunability by tuning the PC, instead of changing the PM fiber length. Fiber birefringence can cause different refractive indexes in the slow and fast axes in PM fibers and random fibers.[36,37] Thus, it can affect the group velocity of the solitons in a vector way, resulting in different spectra and soliton pulse durations in the different fiber axes.[38] The drifting pulses and CP could propagate in different PM fiber axes by adjusting the PC, but a polarization beam splitter would be needed to measure the vector solitons in different fiber axes. The sharp dips in the spectrum are attributed to the intrinsic absorption peaks and molecular resonances of the Tm-doped fiber.[39,40]

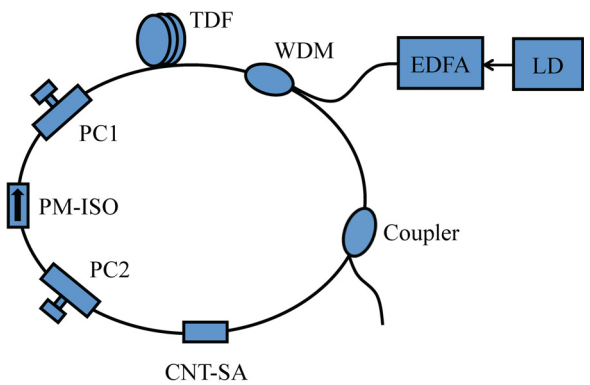

FIG. 1. Fiber laser set-up. LD: laser diode; EDFA: erbium-doped fiber amplifier; WDM: wavelength-division multiplexer; TDF: Tm-doped fiber; PC: polarization controller; PM-ISO: polarization-maintaining isolator; CNT-SA: carbon nanotube-based saturable absorber.

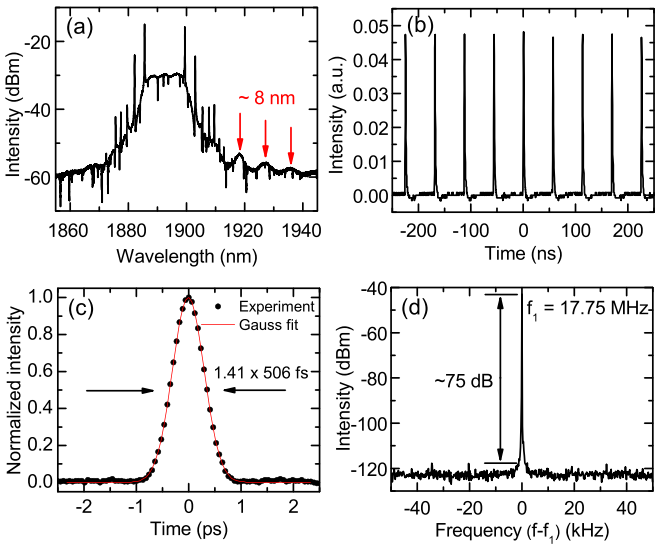

FIG. 2. (a) Optical spectrum, (b) temporal waveform, (c) autocorrelation trace, and (d) RF spectrum.

Figure 2(b) shows the temporal waveform at the fundamental repetition rate (FRR) ~17.75 MHz, corresponding to the cavity length. Figure 2(c) plots the autocorrelation trace. Our laser has a PM-ISO with two PCs for spectral filtering. In this case, Ref. 16 showed that the pulse is close to a Gauss profile. Hence we use this to fit the autocorrelation trace and get FWHM ~506 fs. The time-bandwidth product (TBP) is 0.614, larger than the theoretical value (0.441) for transform-limited Gauss-shaped pulses,[41] indicating minor chirping.[41] The signal-to-noise ratio (SNR) of the radio-frequency (RF) spectrum with a resolution of 10 Hz, Fig. 2(d), is 75 dB (i.e., $10^{7.5}$) at the FRR, indicating stable mode-locking.[42] This is higher than that in Ref. 8, ~50 dB, Ref. 10, ~70 dB, Ref. 38, ~48–58 dB, and Ref. 43, ~60 dB.

By increasing the pump power and adjusting the PCs, we achieve SR. Figure 3(a) plots the SRs oscilloscope trace when we increase the pump power to ~650 mW. The output power is ~43.3 mW. The red arrows indicate CPs that radiate the drifting pulses (blue arrows) from left to right. During the SR process, the drifting pulses spontaneously start from one CP and vanish close to the next CP.[3–8] The spacing of two adjacent CPs is the FRR.[1,2] The central wavelength of the spectrum, Fig. 3(b), is 1884 nm with FWHM ~10.4 nm. Figure 3(c) shows the autocorrelation trace of the soliton pulses. A good fit is obtained by using a Gauss profile, with FWHM ~534 fs. These are solitons in the static state, i.e. the CP. The TBP is ~0.469, close to the theoretical value.[41] The SNR of the RF spectrum with a resolution of 10 Hz, Fig. 3(d), is 60 dB at the FRR, smaller than the mode-locked SNR (~75 dB), due to the soliton flow.[42] The RF spectrum in Fig. 3(e) has fluctuations also due to the soliton flow.[42]

SRs in our laser originate from the CP and drift towards the next CP as shown in Fig. 3(a) (Multimedia view). The drifting speed can be changed by adjusting the PC, since SRs are sensitive to polarization.[1,2] Figures 3(a) and 4(a) (Multimedia view) show the different drifting speeds of the SR2 when PC is tuned at different orientations, with a high resolution image in Fig. 4(b) (Multimedia view). A pulse spacing up to 250 ps can be detected, originating from the

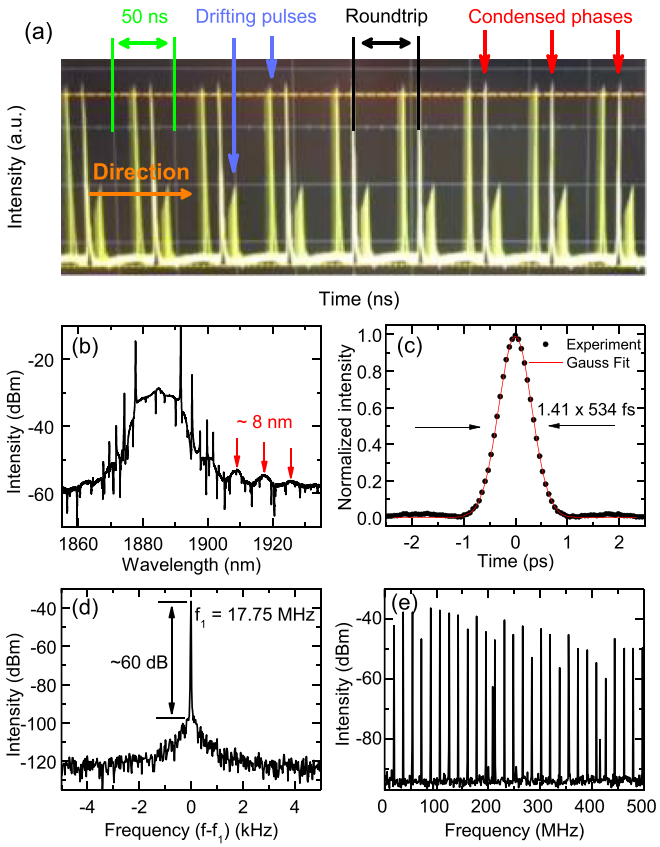

FIG. 3. (a) Oscilloscope trace of SRs, (b) optical spectrum, (c) autocorrelation, (d) RF spectrum, and (e) RF spectrum with a span of 500 MHz. Multimedia view: https://doi.org/10.1063/1.5047492.1

CP. During the process, the amplitudes of the drifting pulses enlarge before they reach the CP, as shown in Fig. 4(b) (Multimedia view). The pulses aggregate energy before they reach the next CP and subsequently release it, i.e. radiate SRs, in dynamic equilibrium. SRs last 10 min if the PC is not used.

By further increasing the pump power and adjusting the PCs, we observe the second- and third-harmonic SRs, Figs. 5(a) and 5(b). Compared to the FRR SR, the CP and the drifting direction of the pulses are unchanged. The drifting pulses still arise from CP and drift from left to right for a roundtrip route, with the amplitude enhanced when they pass

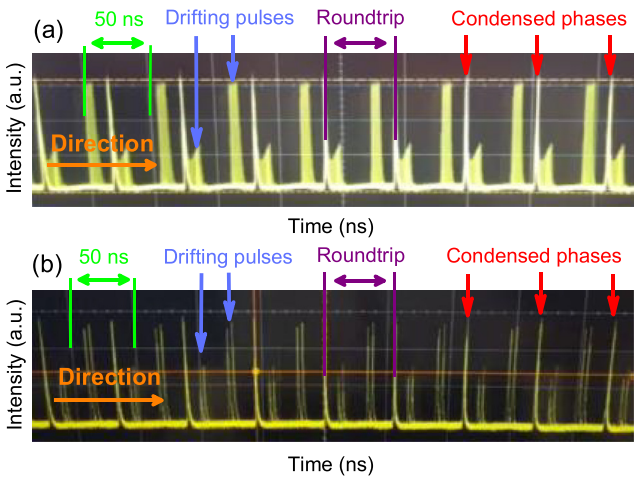

FIG. 4. (a) SR drifting speed and (b) high-resolution image of SR pulses. Multimedia views: https://doi.org/10.1063/1.5047492.2; https://doi.org/10.1063/1.5047492.3

the second- and third-harmonics, due to the superposition of the harmonics and the drifting pulses. The drift speed can be changed by adjusting the PCs since SRs are sensitive to polarization.[4,7,8] Figures 5(c) and 5(d) plot the output wavelengths corresponding to the second- and third-harmonic SRs. The central wavelengths are 1889 and 1892 nm, with FWHM ~14.2 and 14.7 nm, respectively. Figures 5(e) and 5(f) show the autocorrelation traces of the second- and third-harmonic SRs. The FWHM are 545 and 542 fs, by using the Gauss pulse profile, with TBP of ~0.651 and 0.668, respectively, larger than expected for transform-limited Gauss-shaped pulses,[41] indicating chirping.

For SR generation, the drifting pulses move faster than the CP. This means that the SRs have different group velocities than the CP, corresponding to different central wavelengths.[1–3] Thus, the SR spectra always show modulations (i.e. extra optical sidebands in addition to Kelly sidebands[44]) because of the interactions between different SRs and CP central wavelengths.[1–8] In our laser, the PM-ISO along with the two PCs acts as a Lyot birefringence filter,[16] enhancing spectral modulation,[45] which is beneficial for SR generation.[3] Note that our PC+PM-ISO+PC configuration cannot play a role in saturable absorption because the standard nonlinear polarization rotation configuration for mode-locking is "PC+polarization-dependent isolator (PD-ISO)+PC".[43]

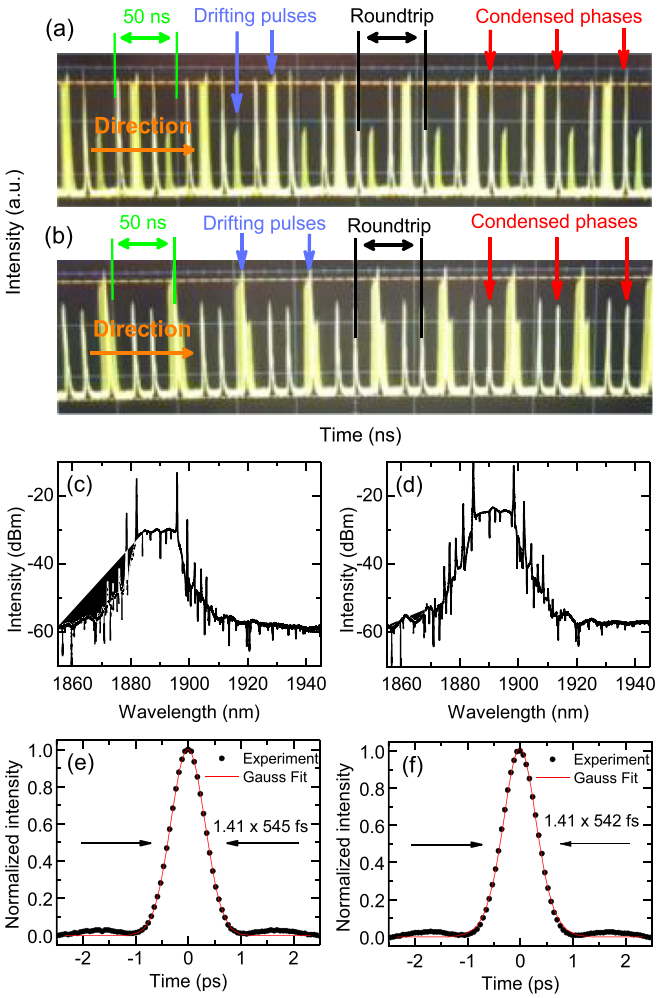

FIG. 5. Oscilloscope traces of (a) second and (b) third-harmonic SRs. Spectra of (c) second- and (d) third-harmonic SRs. Autocorrelation traces of (e) second- and (f) third-harmonic SRs.

PC+PD-ISO+PC can be used as artificial SA because it has weak birefringence, and one can change the light transmission by tuning the PCs. The pigtail of the PD-ISO is a SMF and that of the PM-ISO is a PM fiber, and thus, the PC+PM-ISO+PC system has strong birefringence, and it is hard to change light transmission by tuning the PCs. Therefore, PC+PM-ISO+PC cannot play a role in saturable absorption. We also note that mode-locking cannot be achieved when the CNT-SA is removed, no matter the PC orientation.

By adjusting the PCs, we obtain SR tunability from 1877 to 1933 nm as shown in Fig. 6. When the central wavelength is tuned from 1877 to 1933 nm, the pulse durations change from 527 to 534 fs, as indicated in Table I. There is no much difference for the SR process. SR originate from the CP and drift towards the next CP. The drift speed can be changed by adjusting the PCs since SRs are sensitive to the cavity polarization.[1,2] As indicated in Table I, the central wavelengths are 1877, 1889, 1900, 1915, 1925, and 1933 nm with FWHM ~14.6, 15.2, 3.1, 13.9, 3.5, and 14.1 nm, respectively. We assume Gaussian pulses for 1877, 1889, 1915, and 1933 nm (as confirmed by spectral modulation[16,45]) and sech^2 for 1900 and 1925 nm (as confirmed by the Kelly sidebands[44]). The pulse durations are ~527, 523, 1284, 543, 1233, and 534 fs, corresponding to TBP ~0.655, 0.668, 0.331, 0.617, 0.349, and 0.605, respectively, indicating chirping for the Gaussian pulses and almost transform-limited behavior for the sech^2 ones (~0.315 holding for a transform-limited pulse[41]). The different wavelength and pulse profiles are attributed to the birefringence filter effect.[16,45]

In summary, we reported the fundamental repetition rate, second- and third-harmonic soliton rains in a wavelength tunable (1877–1933 nm) Tm-doped fiber laser mode-locked by carbon nanotubes. The pulse durations of the fundamental, second-, and third-harmonic SRs are ~534, 545, and 542 fs, respectively. The condensed soliton phase and the drifting direction of the pulses are unchanged during the process. This makes our system promising as a tunable filter for ultrafast spectroscopy.

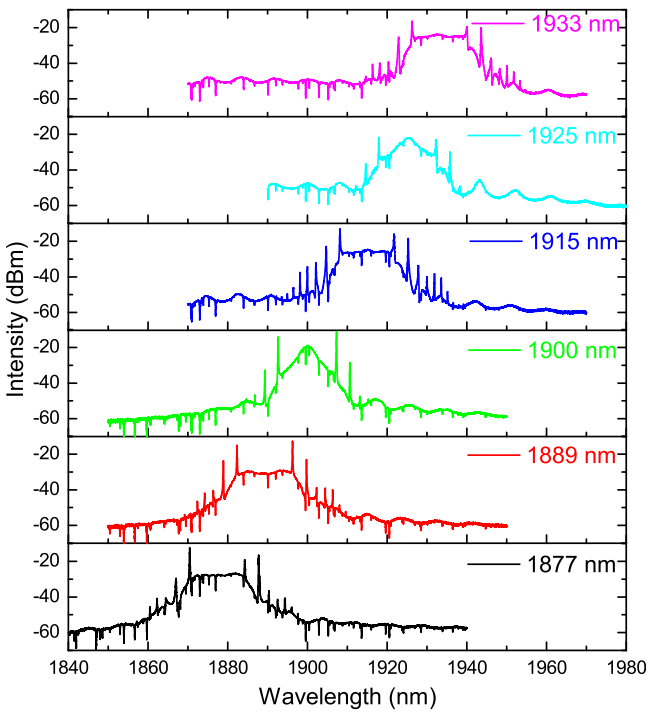

FIG. 6. Wavelength tunable spectra.

TABLE I. Output properties of wavelength tunable spectra.

Wavelength (nm)	FWHM (nm)	Pulse duration (fs)	TBP
1877	14.6	527	0.655
1889	15.2	523	0.668
1900	3.1	1284	0.331
1915	13.9	543	0.617
1925	3.5	1233	0.349
1933	14.1	534	0.605

We acknowledge funding from ERC Grant Hetero2D, EPSRC Grants Nos. EP/L016087/1, EP/K017144/1, EP/K01711X/1 and the China Scholarship Council.

[1]S. Chouli and P. Grelu, Opt. Express **17**, 11776 (2009).
[2]S. Chouli and P. Grelu, Phys. Rev. A **81**, 063829 (2010).
[3]C. Bao, X. Xiao, and C. Yang, Opt. Lett. **38**, 1875 (2013).
[4]S. Huang, Y. Wang, P. Yan, G. Zhang, J. Zhao, H. Li, and R. Lin, Laser Phys. Lett. **11**, 025102 (2014).
[5]C. P. Singh, P. K. Gupta, A. J. Singh, S. K. Sharma, P. K. Mukhopadhyay, K. S. Bindra, and S. M. Oak, IEEE Photonics Technol. Lett. **28**, 1533 (2016).
[6]Y. Meng, S. Zhang, X. Li, H. Li, J. Du, and Y. Hao, Opt. Express **20**, 6685 (2012).
[7]A. Niang, F. Amrani, M. Salhi, P. Grelu, and F. Sanchez, Appl. Phys. B: Lasers Opt. **116**, 771 (2014).
[8]Y. Xu, Y. Song, G. Du, P. Yan, C. Guo, G. Zheng, and S. Ruan, Laser Phys. Lett. **12**, 045108 (2015).
[9]M. E. Fermann and I. Hartl, Nat. Photonics **7**, 1006 (2013).
[10]M. Zhang, E. J. R. Kelleher, F. Torrisi, Z. Sun, T. Hasan, D. Popa, F. Wang, A. C. Ferrari, S. V. Popov, and J. R. Taylor, Opt. Express **20**, 25077 (2012).
[11]L. E. Nelson, E. P. Ippen, and H. A. Haus, Appl. Phys. Lett. **67**, 19 (1995).
[12]B. M. Walsh, Laser Phys. **19**, 855 (2009).
[13]Z. Li, Z. A. M. Heidt, N. Simakov, Y. Jung, J. M. O. Daniel, S. U. Alam, and D. J. Richardson, Opt. Express **21**, 26450 (2013).
[14]N. M. Fried and K. E. Murray, J. Endourol. **19**, 25 (2005).
[15]S. W. Henderson, P. J. M. Suni, C. P. Hale, S. M. Hannon, J. R. Magee, D. L. Bruns, and E. H. Yuen, IEEE Trans. Geosci. Remote Sens. **31**, 4 (1993).
[16]K. Özgören and F. Ö. Ilday, Opt. Lett. **35**, 1296 (2010).
[17]F. Wang, A. G. Rozhin, V. Scardaci, Z. Sun, F. Hennrich, I. H. White, W. I. Milne, and A. C. Ferrari, Nat. Nanotechnol. **3**, 738 (2008).
[18]E. J. R. Kelleher, J. C. Travers, E. P. Ippen, Z. Sun, A. C. Ferrari, S. V. Popov, and J. R. Taylor, Optics Lett. **34**, 3526 (2009).
[19]K. Kieu, Q. Fang, and N. Peyghambarian, IEEE Photonics Technol. Lett. **22**, 1656 (2010).
[20]T. Hasan, Z. Sun, P. Tan, D. Popa, E. Flahaut, E. J. R. Kelleher, F. Bonaccorso, F. Wang, Z. Jiang, F. Torrisi, G. Privitera, V. Nicolosi, and A. C. Ferrari, ACS Nano **8**, 4836 (2014).
[21]Y. Meng, Y. Li, Y. Xu, and F. Wang, Sci. Rep. **7**, 45109 (2017).
[22]Z. Zhang, D. Popa, V. J. Wittwer, S. Milana, T. Hasan, Z. Jiang, A. C. Ferrari, and F. Ö. Ilday, Appl. Phys. Lett. **107**, 241107 (2015).
[23]D. Popa, Z. Sun, T. Hasan, W. B. Cho, F. Wang, F. Torrisi, and A. C. Ferrari, Appl. Phys. Lett. **101**, 153107 (2012).
[24]T. Hasan, Z. Sun, F. Wang, F. Bonaccorso, P. Tan, A. G. Rozhin, and A. C. Ferrari, Adv. Mater. **21**, 3874 (2009).
[25]A. Martinez and Z. Sun, Nat. Photonics **7**, 842 (2013).
[26]O. Okhotnikov, *Fiber Lasers* (Wiley-VCH, Berlin, 2012).
[27]C. A. Zaugg, Z. Sun, V. J. Wittwer, D. Popa, S. Milana, T. S. Kulmala, R. S. Sundaram, M. Mangold, O. D. Sieber, M. Golling, Y. Lee, J. H. Ahn, A. C. Ferrari, and U. Keller, Opt. Express **21**, 31548 (2013).
[28]W. B. Cho, J. W. Kim, H. W. Lee, S. Bae, B. H. Hong, S. Y. Choi, I. H. Baek, K. Kim, D.-I. Yeom, and F. Rotermund, Opt. Lett. **36**, 4089 (2011).

[29]J. Wang, H. Chen, Z. Jiang, J. Yin, J. Wang, M. Zhang, T. He, J. Li, P. Yan, and S. Ruan, Opt. Lett. **43**, 1998 (2018).
[30]J. Wang, Z. Jiang, H. Chen, J. Li, J. Yin, J. Wang, T. He, P. Yan, and S. Ruan, Photonics Res. **6**, 535 (2018).
[31]S. Lebedkin, P. Schweiss, B. Renker, S. Malik, F. Hennrich, M. Neumaier, C. Stoermer, and M. M. Kappes, Carbon **40**, 417 (2002).
[32]F. Hennrich, R. Wellmann, S. Malik, S. Lebedkin, and M. M. Kappes, Phys. Chem. Chem. Phys. **5**, 178 (2003).
[33]S. Osswald, E. Flahaut, and Y. Gogotsi, Chem. Mater. **18**, 1525 (2006).
[34]K. Liu, J. Deslippe, F. Xiao, R. B. Capaz, X. Hong, S. Aloni, A. Zettl, W. Wang, X. Bai, and S. G. Louie, Nat. Nanotechnol. **7**, 325 (2012).
[35]J. Zhao, L. Li, L. Zhao, D. Tang, and D. Shen, Opt. Lett. **43**, 247 (2018).
[36]D. N. Christodoulides and R. I. Joseph, Opt. Lett. **13**, 53 (1988).
[37]S. T. Cundiff, B. C. Collings, N. N. Akhmediev, J. M. Soto-Crespo, K. Bergman, and W. H. Knox, Phys. Rev. Lett. **82**, 3988 (1999).
[38]L. Yun, Opt. Express **25**, 18751 (2017).
[39]A. Stark, L. Correia, M. Teichmann, S. Salewski, C. Larsen, V. M. Baev, and P. E. Toschek, Opt. Commun. **215**, 113 (2003).
[40]G. Sobon, J. Sotor, I. Pasternak, A. Krajewska, W. Strupinski, and K. M. Abramski, Opt. Express **23**, 9339 (2015).
[41]G. P. Agrawal, *Applications of Nonlinear Fiber Optics* (Academic Press, London, 2001).
[42]D. von der Linde, Appl. Phys. B **39**, 201 (1986).
[43]P. Wang, C. Bao, B. Fu, X. Xiao, P. Grelu, and C. Yang, Opt. Lett. **41**, 2254 (2016).
[44]S. M. J. Kelly, Electron. Lett. **28**, 806 (1992).
[45]G. E. Villanueva and P. Pérez-Millán, Opt. Lett. **37**, 1971 (2012).